Photoionization of the hydrogen 4s state by a strong laser pulse: Bare-state dynamics and extended-charge-cloud oscillations

K. Im, R. Grobe, and J. H. Eberly
Department of Physics and Astronomy, University of Rochester, Rochester, New York 14627
(Received 24 June 1993)

The response of a hydrogen atom initially prepared in the 4s state and subjected to a short, intense laser pulse is studied by calculating field-dependent time-dependent wave functions numerically as a function of r and θ. We calculate the probabilities of bound states that are dipole connected to the 4s state both directly and by two-photon Raman coupling through the continuum. We find that for intensities in the neighborhood of 10^{15} W/cm^2 the bound states exchange population relatively slowly in time while ionizing. Space-time plots of the electronic charge cloud show a complex but very stable extended microstructure like that of a stabilized polychotomous wave packet. A calculation of the expectation value of the charge cloud's position along the axis of laser polarization shows behavior similar to free-electron behavior although the extent of the charge cloud is much greater than the free-electron oscillation amplitude.

PACS number(s): 32.80.Rm, 42.50.Hz

I. INTRODUCTION

Beginning in the 1970s a number of authors suggested that a qualitative change in the atomic photoionization process might be expected if super-strong laser fields became available. Specifically, a counterintuitive decrease of the photoionization rate was predicted to accompany an increase of the laser field strength by Geltman and Teague [1], Gersten and Mittleman [2], and by Gavrila and co-workers [3] in their work on the hydrogen atom in the Kramers-Henneberger (KH) frame [4]. They forecast the existence of an asymptotic high-frequency and high-intensity regime in which the photoionization rate would be inversely proportional to field strength. Localization and stabilization of the atomic electron in a new type of lowest-energy orbit were also predicted [3]. It has been demonstrated in numerical experiments [5] that the same phenomena can also be expected in a pulsed laser field with a finite turn-on time, and more recently that this can occur with values of frequency and intensity that are not asymptotic but even within the range of currently available lasers [6]. Ionization suppression and atomic stabilization have subsequently been discussed in other contexts as well: a classical atom [7], i.e., an atom initially in a Rydberg level [8–10] or in a low-lying excited state [11,12].

Several mechanisms for stabilization have been proposed in these studies: field-induced wide-scale free-electron oscillations outside the influence of atomic binding [1–6], interference occurring between ionization channels from neighboring Rydberg states [8,9], and electron trapping in excited states associated with the formation of a spatially extended wave packet [10]. Although several reviews of stabilization are now available [13,14], the detailed relationships among the various possible mechanisms have not been resolved at this time. For example, an open issue concerning Rydberg interference and wave-packet stabilization is the relevance of the so-called Kramers-Henneberger parameter α, which is the amplitude of oscillation of a nonrelativistic free electron in a laser field. That is, if the electric field of the laser is $E(t)=\mathcal{E}_0\sin\omega t$, then the free-electron response is $x(t)=\alpha\sin\omega t$, where (in atomic units)

$$\alpha=\mathcal{E}_0/\omega^2 . \tag{1.1}$$

Part of our motivation here is to look for evidence for free-electron or KH stabilization and a possible role for α when the initial state is one of a close manifold of states susceptible to one-photon ionization. This is the regime in which Rydberg interference, Raman mixing, and wave-packet formation can also be expected. The ultimate motivation for studying initial excited states is that one-photon ionization can be achieved at optical frequencies, making proposed experiments more realistic. Optical one-photon ionization is possible from excited states of hydrogen at or above $n=3$. Our paper can be regarded as an expansion of the earlier strong-field studies of low-lying excited states in hydrogen by Piraux, Knight, and co-workers [11] and Pont and Shakeshaft [12]. For example, we use the expectation value of the electron position along the axis of laser polarization to provide quantitative evidence that the KH parameter α plays an important role in excited-state dynamics. We also find that a comparison of the Kepler period with the periodic exchange of population between neighboring excited states casts some doubt on the general relevance of two-photon Raman mixing as an ionization-suppression and stabilization mechanism.

We have chosen the 4s state as the initial state. It has an orbital radius an order of magnitude greater than the Bohr radius a_0 but is not yet in the quasiclassical regime of states employed in the studies of Fedorov and Stroud and their collaborators [8,10]. We have calculated 3s, 4s, 4p, 4d, and 5s and other excited-state probabilities during and after a strong laser pulse, as well as space-time probability distributions.

II. METHOD OF SOLUTION OF SCHRÖDINGER'S EQUATION

We work with the time-dependent Schrödinger equation for the hydrogen atom in an external field

$$i\frac{\partial\psi(\mathbf{r},t)}{\partial t}=[H_0(r)+H_I(\mathbf{r},t)]\psi(\mathbf{r},t)\ , \tag{2.1}$$

where the atomic Hamiltonian is

$$H_0(r)=-\tfrac{1}{2}\nabla^2-\frac{1}{r}\ . \tag{2.2}$$

We can speak of each solution of Schrödinger's equation as a numerical experiment. In these equations and throughout the paper we use atomic units with $e=m=\hbar=1$. The interaction Hamiltonian is, in the dipole approximation,

$$H_I(\mathbf{r},t)=\mathbf{r}\cdot\mathbf{E}(t)\sin\omega t\ , \tag{2.3}$$

where ω is the laser frequency. We consider a laser linearly polarized along the z axis, $\mathbf{r}\cdot\mathbf{E}(t)=r\cos\theta\mathcal{E}(t)$, where the field envelope $\mathcal{E}(t)$ is chosen as a trapezoidal pulse that is linearly turned on and off over two optical cycles. If spherical coordinates are utilized [15], the time-dependent wave function can be expanded as a function of only two spatial coordinates r and θ:

$$\psi(\mathbf{r},t)=\sum_{l=0}^{L}\frac{1}{r}\chi_l(r,t)Y_l^0(\theta)\ . \tag{2.4}$$

The azimuthal quantum number ($m=0$ when starting in an S state) is conserved for linearly polarized light.

The radial part of the wave function has been integrated in time using the Crank-Nicholson method on a spatial grid. The maximum radius was 400 a.u. and the wave function was smoothly cut off for radii larger than 200 a.u. to prevent reflection of the wave function at the boundary. The norm of the wave function decreases with time, but the bound-state probabilities are scarcely affected by the cutoff because the dynamically important bound states are localized at smaller radii. It was sufficient for our calculations to restrict the maximum angular momentum to $L=127$. The time step and the radial grid have been chosen to achieve an overall calculation error below 5%.

Some comments can be helpful in understanding the reliability of calculations of this type, which with small variations have been made repeatedly in carrying out numerical experiments on hydrogen in strong fields [13]. First of all, one recognizes that since the calculation is made in a large box of several hundred a.u. radius with the localized $1/r$ potential of range 1 a.u. at the origin, the radial eigenfunctions of the box used in the calculation are not the same as the infinite-space eigenfunctions of hydrogen. Nevertheless, within the box these eigenfunctions provide a complete orthonormal basis and can be used for expanding the wave function exactly, and for following its time evolution exactly. The failure of the box method comes, of course, whenever the electron wave packet moves close to the walls of the box. This is easy to monitor, and one mostly needs to guard against reflections. When carrying out such calculations it is important to be prepared for several phenomena common to high-intensity numerical experiments that are not part of the "conventional wisdom" of usual photoionization theory. The most striking example is the unconventional character of the electron motion. Since the laser's electric field is so effective in moving the electron back and forth (quiver motion), it is not a sure sign of ionization to find a positive-energy electron during the laser pulse. We show below, in common with prior calculations, that the electron wave function can have zero overlap with its bound eigenstates *in a periodic fashion.* That is, using conventional language, one would say that the same electron becomes ionized and then returns to the atom many times in rapid succession. As regards angular momentum, rather high values may be needed to account accurately for the elongation of those parts of the electron packet that are undergoing extended quiver motion. In considering maximum l values one may think that the $\Delta l=1$ selection effectively restricts how high an l value can be reached, starting from $l=0$, but it is not much help since the laser pulse contains about 10^5 photons. As we mentioned, the upper limit $l=127$ is adequate. However, one should not jump to the conclusion that the need for $l=127$ implies that Rydberg states with $n\geq 128$ are being substantially populated. In fact, in a box of conventional size it is unusual to have 128 bound states in the $1/r$ potential, so states with large n are actually positive-energy states and again one must realize that population of positive-energy states during the pulse does not equate to ionization.

III. LEVEL POPULATION RESULTS

One of our typical numerical experiments begins with the hydrogen atom in its $4s$ state. It is then subjected to an interaction with a linearly polarized 20-cycle laser pulse with maximum field strength $\mathcal{E}_0$. This numerical experiment is repeated for several field strengths. The laser frequency is fixed at the high value $\omega=0.30$ a.u. in all the calculations. This is primarily for computational reasons, but it also avoids resonances with other bound states above and below $4s$ and allows for single-photon ionization well above the threshold. These features of our study are summarized in the energy-level diagram in Fig. 1.

In Fig. 2 we show several population trends as a function of laser peak intensity: the $4s$ population (circles), the total bound-state population (squares), and also the norm of the final wave function (diamonds), all calculated after the 20-cycle pulse was turned off. The dashed line shows the corresponding Fermi golden rule rate Γ obtained from the standard photoionization rate formula, specifically,

$$\Gamma=\frac{\pi}{2}|\langle 4s|r\cos\theta\mathcal{E}_0|E\rangle|^2\rho(E)\ , \tag{3.1}$$

where $E=E_{4s}+\omega$. Under the conditions of our numerical integration the density of states at the one-photon ionized state (0.27 a.u. above the ionization threshold) is about 170 a.u. and formula (3.1), in the present case, reduces to

$$\Gamma=0.16\mathcal{E}_0^2\ . \tag{3.2}$$

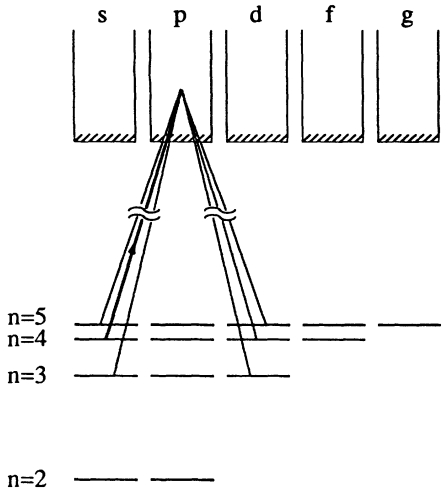

FIG. 1. Sketch of hydrogen energy levels (not to scale) showing the relation to the laser frequency and the transitions of main interest.

The final bound-state probabilities obtained in these numerical experiments at first decrease rapidly with intensity, in good agreement with the Fermi golden rule prediction at low field strengths, as is clearly evident in Fig. 2. We also notice that the total bound-state probability is about twice the final 4*s*-state probability, for all field strengths at and above the value $\mathcal{E}_0=0.21$ a.u. ($I\approx 1.5\times 10^{15}$ W/cm^2).

On an expanded vertical scale, Fig. 3 shows the final probabilities of several of the other bound states near to the initial state as a function of intensity. At intensities less than 10^{15} W/cm^2 almost none are populated except the initial state. As the intensity increases, the 5*s* state gets populated preferentially. In Figs. 4 and 5 we show the various level probabilities as a function of time, obtained by projecting the exact wave function onto various bare states. Some difficulties of interpretation of time-dependent midpulse quantities are well known, but they

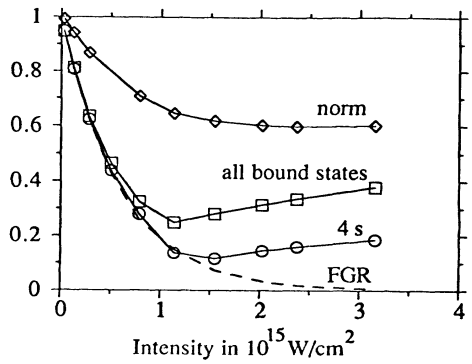

FIG. 2. Initial (4*s*)-state probability and its Fermi golden rule prediction, the total bound-state probability, and the norm of the final wave function after a 20-cycle pulse of frequency $\omega=0.3$ a.u. The wave function was smoothly cut off for radii larger than 200 a.u. and the norm of the wave function decreases as the field intensity increases up to about 1.4×10^{15} W/cm^2, above which the atom stabilizes.

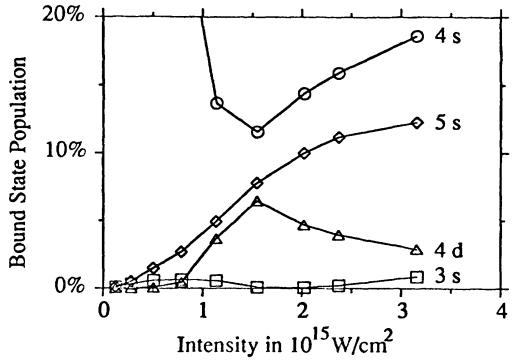

FIG. 3. The dependence of bound-state probabilities on the field intensity for the 4*s*, 5*s*, 4*d*, and 3*s* states for a 20-cycle pulse with $\omega=0.3$ a.u. A portion of the curve belonging to the 4*s* state is not shown in this scale.

can nevertheless offer some useful insights [16,17]. Close inspection of Fig. 4 shows that all levels have zero population almost all of the time. It is only very close to the quarter-cycle and three quarter-cycle time points that there is apparently any population in the bound levels at all. The envelopes of these curves show, however, what is confirmed in Fig. 5 over a longer interval, that there is a relatively slow oscillation of probability between the nearby *s* levels. The irregular changes in the envelopes of the curves at 2 cycles and 18 cycles are due to the trapezoidal pulse shape used in our simulation.

IV. EVIDENCE FOR STABILIZATION FROM LEVEL POPULATIONS

First we focus on KH stabilization. The rapid oscillations and their timing, shown in Fig. 4, are very similar to those found in the first numerical studies of pulsed-laser ground-state stabilization [5], and can be given the same interpretation [17,18]. The very brief moments of nonzero level populations shown in all curves in Fig. 4 occur when the electron is subjected to *maximum* laser field strength [recall the phase of the field in Eq. (2.3)]. If the electron is free, this is the time it is located at the farthest position from the nucleus before the field begins to pull it back. At that location its wave function has the largest overlap with the initial 4*s* state because it has its longest de Broglie wavelength there (where the free-electron velocity is zero). At other times, when it is physically closer to the nucleus, it has a very highly oscillatory wave function (it is moving rapidly) and can't have a large wave function overlap with the 4*s* state. This type of behavior is one key to KH stabilization.

A further suggestion of stabilization is evident in the curve showing the population of all bound states in Fig. 2, as the ionization rate trend clearly reverses for $\mathcal{E}_0>0.18$ a.u., i.e., for intensities higher than about 10^{15} W/cm^2. This "critical" intensity [19] corresponds to a KH parameter with the value $\alpha=2$ a.u., and the ionization rate reversal is consistent with data obtained by Pont and Shakeshaft [12] from Gaussian pulses of five-cycle full width at half maximum (FWHM) with $\omega=0.2$ a.u. and $\mathcal{E}_0\approx 0.17$ a.u.

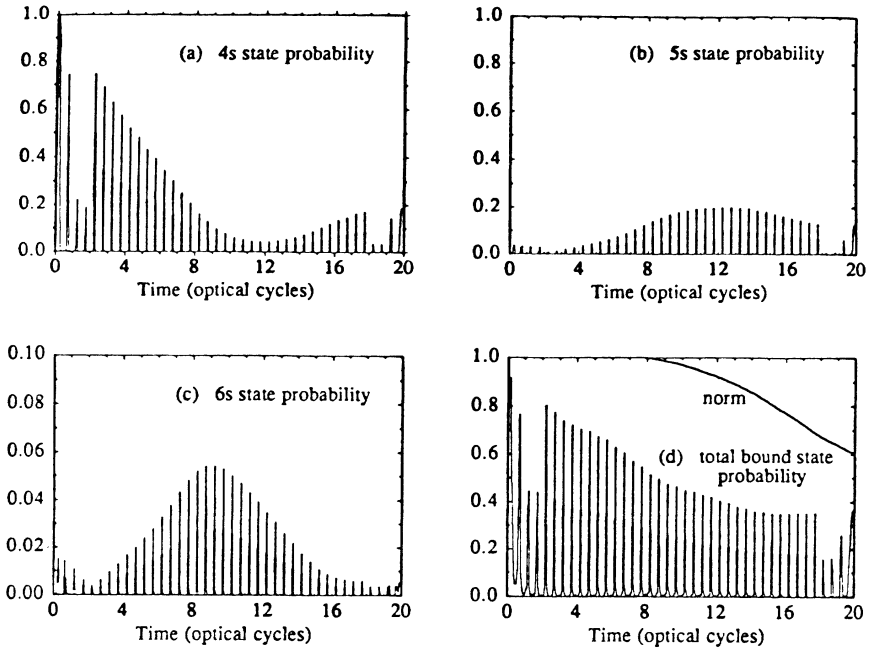

FIG. 4. Time-dependent bound-state probabilities of the 4*s*, 5*s*, and 6*s* states. The total bound-state probability and the time-dependent norm are also drawn. The field is $\mathcal{E}_0=0.30$, corresponding to laser intensity $I\approx 3\times 10^{15}$ W/cm^2, for all curves.

Let us turn our attention to the features associated with Rydberg-interference or wave-packet stabilization. There are two critical intensities associated with the stabilization domain proposed by Fedorov and his coworkers [8]. The lower critical intensity is reached when the ionization-induced broadening of the Rydberg levels is comparable to the nearest-neighbor level spacing. At a less well-defined higher critical intensity the broadened and overlapping Rydberg levels should separate from each other and their widths should get smaller with increasing intensity. We can compute $\Gamma=0.0052$ a.u. from (3.2), given the field strength $\mathcal{E}_0=0.18$ a.u. that appears to be critical on the basis of Fig. 2. The level spacing δ has the value 0.011 a.u. between the 4*s* state and the 5*s* state (which in the present calculation is the state with the second largest population after the initial 4*s* state). Thus we obtain the value $\Gamma/\delta=0.47$, indicating that ionization-broadened overlap is minimal at best, and arguing against the relevance of Rydberg-interference stabilization under these conditions.

For only slightly higher values of $\mathcal{E}_0$ we do find bound-state population redistribution, which might be considered consistent with the onset of Rydberg-interference stabilization. However, it could also have another origin. There is a spectral width $\Delta\omega\approx 0.015$ a.u. connected with the laser linewidth of the present 20-cycle pulse, which is slightly larger than the 4*s*-5*s* spacing of $\delta=0.011$ a.u., so the 5*s* state is effectively in near two-photon resonance with 4*s*, independent of any ionization broadening. The final-time populations of the 4*s* and 5*s* states first become comparable at $\mathcal{E}_0=0.21$ a.u. ($I\approx 1.5\times 10^{15}$ W/cm^2). The population of the 4*d* state closely follows the 5*s* population up to about the same point, but decreases as the field strength increases further. The population of the 3*s* state shows a small variation with the change of field strength. Other bound-state probabilities also have similar features. The reasons for these details of level population behavior are not known at present.

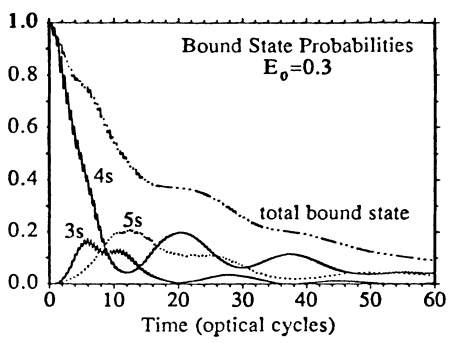

FIG. 5. The envelopes of the time-dependent bound-state probabilities of the 3*s*, 4*s*, and 5*s* states, corresponding to the curves shown in Fig. 4, for a longer time.

Now recall the time evolution of the bound-state probabilities for 4*s*, 5*s*, and 6*s* states as shown in Figs. 4 and 5. An oscillatory behavior of the probabilities of Rydberg states has been discussed for an initially excited hydrogen atom in strong laser field [10]. Given a well-localized Rydberg wave packet, the most rapid ionization rate of the initial Rydberg state can be seen to be the inverse of one Kepler period. This is based on the view that ionization occurs only when the electron passes near the nucleus (i.e., when the electron is accelerated). For such an electronic wave packet exposed to a long laser pulse, the total bound-state population should decrease in a stepwise way, a bit more of it becoming ionized with every transit of the packet past the nucleus.

Our data contains such steps and they are consistent with a wave-packet viewpoint if we adopt [without real justification at $n=4$] the high-Rydberg formula for the Kepler period $T_K=2\pi n^3$. In our case one optical period is $2\pi/\omega=20.9$ a.u., so $T_K\approx 402$ a.u. is about 20 laser cycles, and the data shown in Fig. 5 extends to about three

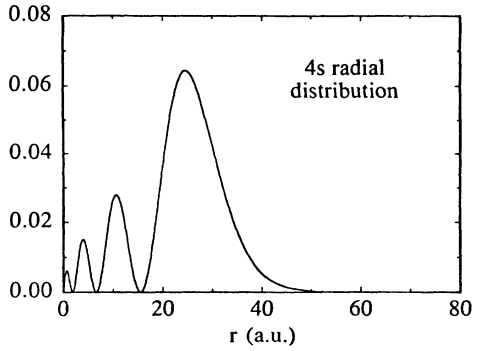

FIG. 6. The radial distribution of electron probability for the initial 4s state.

Kepler periods. It is apparent that steps in the total bound-state probability curve can be seen, and they have the right interval, slightly less than 20 optical cycles. In addition, in both Figs. 4 and 5 the times for the minima and maxima of the 4s-state probability roughly coincide with the times for maxima and minima of the 5s-state probability, and these both occur with about half of the Kepler period. If one concludes that some spatio-temporal wave-packet "coherence" has built up, it is clear that it was induced in the atom while undergoing ionization, since none was present with the initial wave function. This is consistent with the view that the ionization process itself will automatically filter out the parts of the wave function that cannot be "stabilized" or "trapped." (At lower field strengths, the minimum time for the 4s-state probability tends to be longer while the time for the 5s maximum remains almost independent of the field strength, and this has not been explained.)

V. RADIAL DISTRIBUTION OF PROBABILITY

The spatial evolution of the electron wave function is as interesting as the temporal evolution. In Fig. 6 we show a 4s wave packet for the bare atom before the laser is turned on. The mean radial distances $\langle r \rangle_n = (3/2)n^2$ for the 4s and 5s states are 24 and 37.5 a.u., respectively. In Fig. 7 we show the effect of laser excitation on the radial distribution. The curves are proportional to the electron's radial probability distribution $P(r)$, where $\int P(r)dr = 1$, i.e.,

$$P(r) = \int \int |\psi(r,\theta,\phi)|^2 r^2 \sin\theta \, d\theta \, d\phi \ . \tag{5.1}$$

The six different graphs in Fig. 7 correspond to six different times near the middle of our 20-cycle laser pulse, for $\mathcal{E}_0 = 0.3$ a.u. The left-hand column shows the radial distribution at the "zero-field" times 9.50, 10.00, and 12.00 cycles after turn on, and the right-hand column shows the distribution for the "maximum field" times exactly one-quarter period later, at 9.75, 10.25, and 12.25 cycles.

All of the graphs in Fig. 7 show essentially the same gross structure, with similar peaks located at approxi-

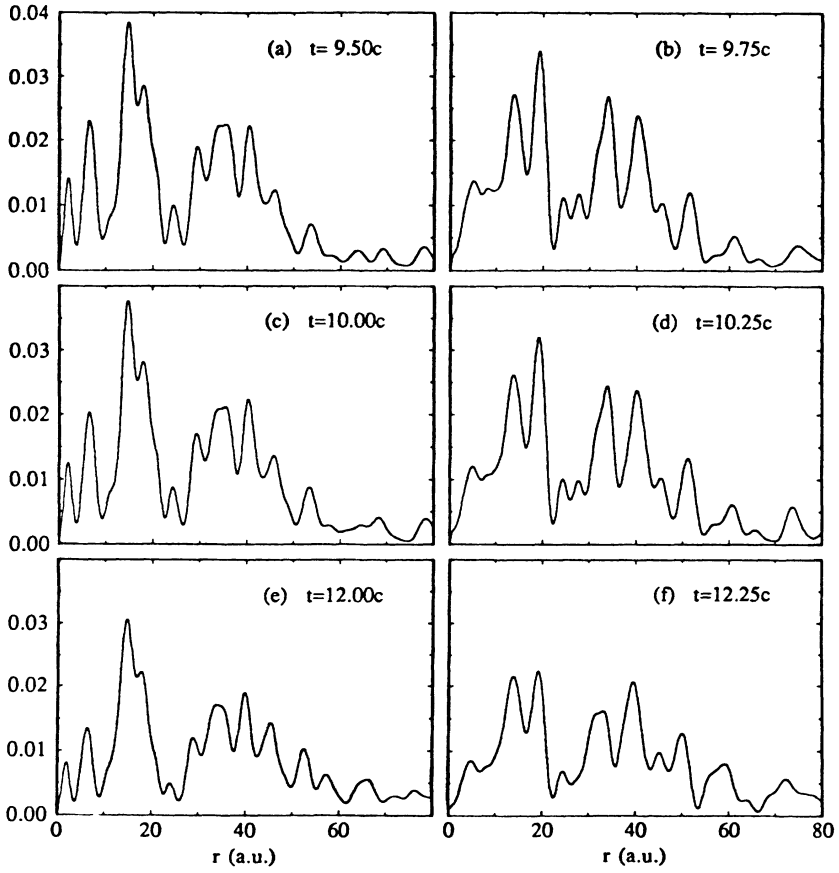

FIG. 7. The electron's radial probability distribution for six different times around the middle of the laser pulse, for $\mathcal{E}_0 = 0.3$ a.u. and $\omega = 0.3$ a.u. Note the striking similarity of curves *a*, *c*, and *e* among themselves and also the similarity of curves *b*, *d*, and *f*.

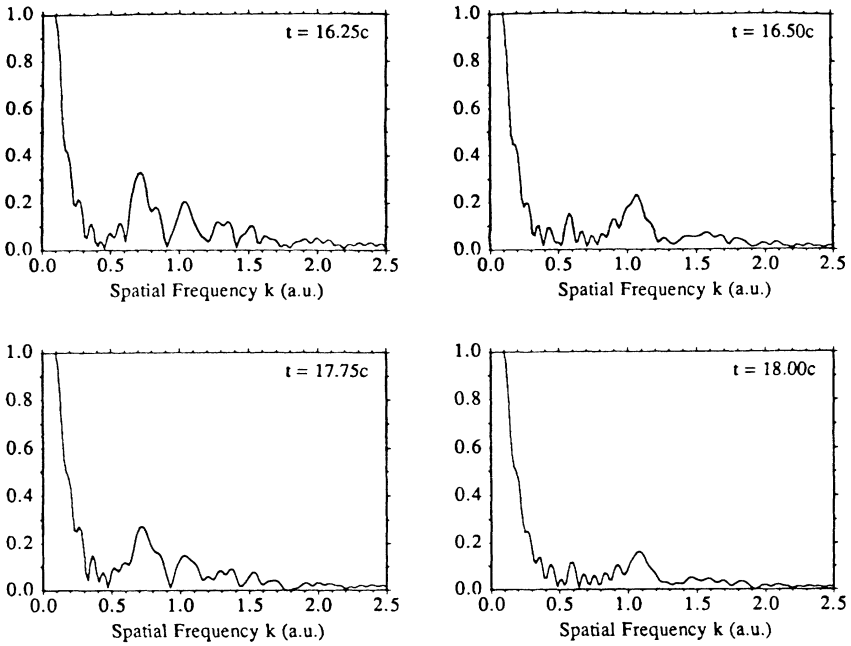

FIG. 8. The spatial Fourier transform of the radial distribution at later times, showing that the clear distinction among the distributions at quarter-cycle and half-cycle times is well preserved during the pulse.

mately the same positions in all figures. The complexity of the spatial forms can be attributed to interferences among bare states, of course. However, this overlooks the point that the complicated spatial forms are strikingly stable. Stability persists despite the fact that during the time interval covered, 9.50 to 12.25 cycles, the bare atomic populations are changing rapidly. For example, during these three cycles the population of the $4s$ state changes by a factor of 2 (recall Fig. 5).

We can also see that, in addition to their overall stability, Figs. 7(a), 7(c), and 7(e) even share most of their detailed features to a remarkable degree, and they differ noticeably from Figs. 7(b), 7(d), and 7(f), which also share a similar microstructure. The stability of the two differing microstructures is impressive. We have calculated spatial Fourier transforms of the radial distribution (between $r=20$ and 80 a.u.), shown in Fig. 8, which confirm the alternation of two spatial forms until the pulse turn off at $t=18c$. It is clear that the radial distributions are undergoing a periodic subtle change of the shape with half the laser period. Neither the shape nor the change has a well-established origin, although they are both reminiscent of the behavior of the stable polychotomous packets obtained by Su [14] and those featured in the report of Reed, Knight, and Burnett [20]. Note, however, that in the present case, $\alpha \approx 3.3$ and the extent of the spatial packet of Fig. 7 is an order of magnitude larger than that.

VI. CYLINDRICAL DISTRIBUTION OF PROBABILITY

Radial distributions do not provide an optimum orientation toward the data, in the sense that spherical (radial) symmetry is a property of the noninteracting hydrogen atom. A more natural view, in the case that field-dependent effects are of main interest, is associated with cylindrical coordinates. Since the selection rule $\Delta m=0$ is strictly obeyed under linear polarization our wave functions are all independent of ϕ, and the appropriate variables are ρ and z. Thus we show three-dimensional representations in Fig. 9 of two snapshots of the square of the wave function $|\psi(\rho,z,\phi;t)|^2$ in the $y=0$ plane, where $\rho \equiv |x|$, at the times $t=17.25$ and 17.75, near the end of the pulse. The existence of a gross oscillation of the elec-

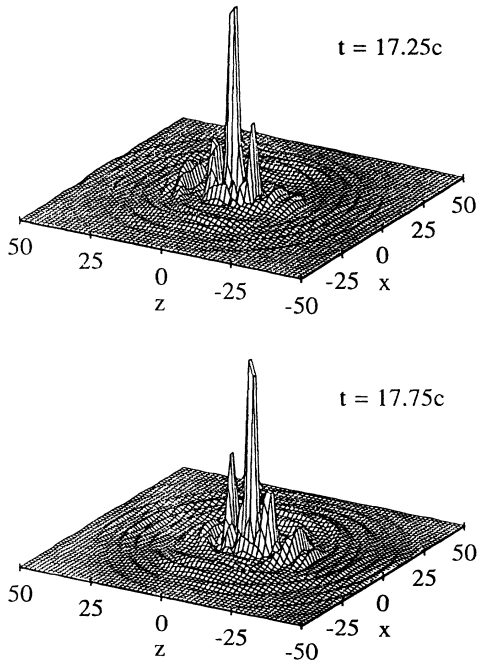

FIG. 9. The absolute square of the wave function for two quarter-cycle times, showing the strong oscillation of the electronic charge cloud.

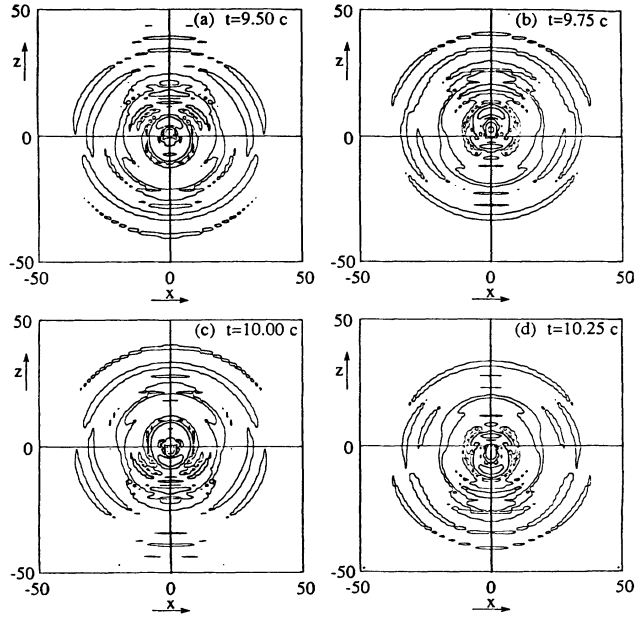

FIG. 10. The square of the wave function $P(\rho,z,t)=|\psi|^2$ plotted in the $y=0$ plane, where $\rho=|x|$, at the same times and under the same conditions as Figs. 7(a)–7(c).

tronic charge distribution between these two times, along the axis of the laser polarization, is obvious.

In Fig. 10 we show the same type of probability distribution as contour plots. We label the distribution $P(x,z;t)$, and it is normalized to unity upon integration over the $x>0$ portion of any of the contour plots, with the volume element $2\pi x\,dx\,dz$. From Fig. 10 we can easily see the details of the spatial structure that makes the graphs in Figs. 7(a), 7(c), and 7(e) similar to each other and distinct from the equally similar graphs in Figs. 7(b), 7(d), and 7(f). Comparison of Figs. 10(a) and 10(c) shows that, for all practical purposes, they are mirror reflections of each other in the $z=0$ line. The same is true of Figs. 10(b) and 10(d), which are nevertheless easily distinguished from Figs. 10(a) and 10(c).

Finally, we analyze directly the oscillation of electronic charge by calculating $\langle z(t)\rangle$, the expectation value of the electron's position coordinate along the field polarization. The result, shown in Fig. 11, clearly indicates that the dynamics are very close to being entirely classical. The am-

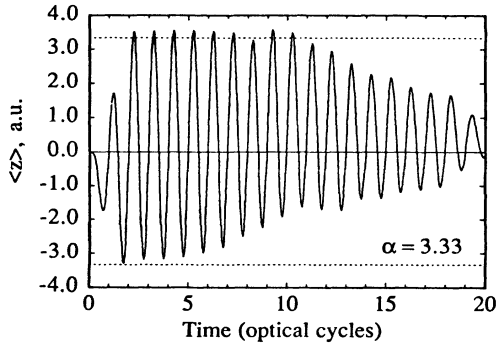

FIG. 11. The expectation value of the component of the electron's position along the laser polarization axis as a function of time. The dotted lines indicate the classical free-electron amplitude of oscillation at $\langle z\rangle=\alpha=3.33$ a.u.

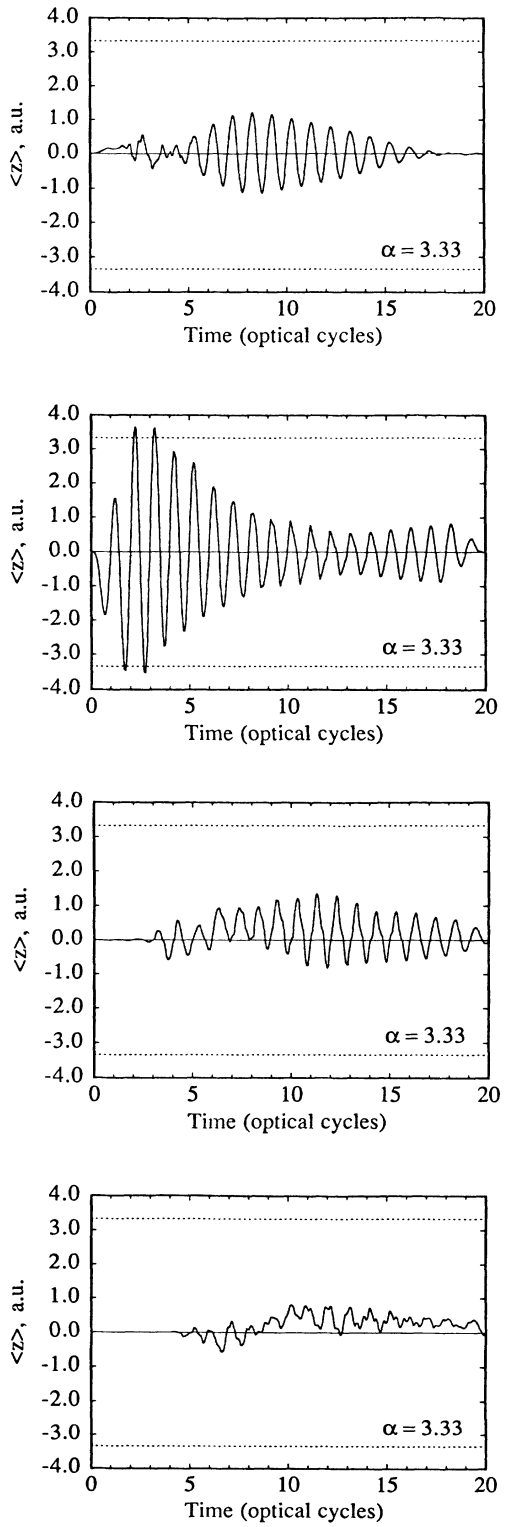

FIG. 12. Contribution to the expectation value $\langle z(t)\rangle$ from different radial regions (from top to bottom): (a) $0<r<R/8$, (b) $R/8<r<R/4$, (c) $R/4<r<R/2$, and (d) $R/2<r<R$; with $R=150$ a.u.

plitude of oscillation is almost exactly equal to $\alpha=\mathcal{E}/\omega^2=3.33$ a.u. until removal of probability at the grid boundary begins to decrease the norm. A slow movement of population among bare states has been shown in Fig. 5 and this also affects $\langle z(t)\rangle$. In Fig. 12 we show the contributions to $\langle z(t)\rangle$ from different radial regions. The response is initially greatest in the region where the charge is initially concentrated, and the response slowly moves both inward and outward as stabilization becomes established. It is clear that the asymmetry in Fig. 11 is due to the asymmetric drifting of the outer (ionizing) fraction, as evident in Figs. 12(c) and 12(d).

VII. SUMMARY

To summarize, we have shown that high-frequency photoionization of a hydrogen atom prepared initially in the 4*s* state begins to be suppressed at a field strength around $\mathcal{E}_0=0.2$ a.u. ($I\approx 1.4\times 10^{15}$ W/cm^2), and this is accompanied by a redistribution of population over other bound states near to the initial 4*s* state. Primarily the 4*s* and 5*s* states are populated, and this population is exchanged quasiperiodically in time. This exchange is accompanied by the formation of an electronic charge cloud with a strikingly stable microstructure. The space-time oscillation of this charge cloud is predicted quantitatively accurately by KH theory. We believe this to be the first evidence that the classical free-electron picture behind KH theory applies quite well to the extended charge distributions of excited states, even when the KH amplitude is much smaller than the extent of the distribution. A number of questions about the details of the dynamics remain open, however, and it appears desirable to analyze the same 4*s* photoionization process directly in the KH frame.

ACKNOWLEDGMENTS

This research was primarily supported by the Division of Chemical Sciences, Office of Basic Energy Sciences, Office of Energy Research of the U.S. Department of Energy. K.I. is also supported by the Ministry of Education in Korea. One of us (R.G.) acknowledges support from the Feodor Lynen Research Fund of the Alexander von Humboldt Foundation of Germany. We are pleased to acknowledge discussions of the interpretation of our experiments with S. Haan and M. V. Fedorov and assistance with the manuscript from D. Lappas and Q. Su.

[1] S. Geltman and M. R. Teague, J. Phys. B **7**, L22 (1974).
[2] J. I. Gersten and M. Mittleman, J. Phys. B **9**, 2561 (1976).
[3] M. Gavrila and J. Kaminski, Phys. Rev. Lett. **52**, 613 (1984); M. Pont, N. R. Walet, M. Gavrila, and C. W. McCurdy, *ibid.* **61**, 939 (1988).
[4] W. C. Henneberger, Phys. Rev. Lett. **21**, 838 (1968); C. K. Choi, W. C. Henneberger, and F. C. Sanders, Phys. Rev. A **9**, 1895 (1974); H. A. Kramers, *Collected Scientific Papers* (North-Holland, Amsterdam, 1956), p. 262.
[5] Q. Su, J. H. Eberly, and J. Javanainen, Phys. Rev. Lett. **64**, 862 (1990); K. C. Kulander, K. J. Schafer, and J. L. Krause, *ibid.* **66**, 2601 (1991).
[6] J. H. Eberly, Phys. Rev. A **42**, 5750 (1990); C. K. Law, Q. Su, and J. H. Eberly, *ibid.* **44**, 7844 (1991); K. C. Kulander, K. J. Schafer, J. L. Krause, and J. H. Eberly (unpublished).
[7] R. V. Jensen and B. Sundaram, Phys. Rev. Lett. **65**, 1964 (1990); J. Grochmalicki, M. Lewenstein, and K. Rzazewski, *ibid.* **66**, 1038 (1991); R. Grobe and C. K. Law, Phys. Rev. A **44**, R4114 (1991); M. Gajda, J. Grochmalicki, M. Lewenstein, and K. Rzazewski, *ibid.* **46**, 1638 (1992).
[8] M. V. Fedorov and A. M. Movsesian, J. Phys. B **21**, L155 (1988); J. Opt. Soc. Am. B **6**, 928 (1989); M. V. Fedorov and M. Yu. Ivanoff, *ibid.* **7**, 569 (1990).
[9] L. Roso-Franco, G. Orriols, and J. H. Eberly, Laser Phys. **2**, 741 (1992).
[10] J. Parker and C. R. Stroud, Jr., Phys. Rev. A **41**, 1602 (1990); M. V. Fedorov, M. Yu. Ivanov, and A. M. Movsesian, J. Phys. B **23**, 2245S (1990).
[11] K. Burnett, P. L. Knight, B. R. M. Piraux, and V. C. Reed, Phys. Rev. Lett. **66**, 301 (1991); B. R. M. Piraux, E. Huens, and P. L. Knight, Phys. Rev. A **44**, 721 (1991).
[12] M. Pont and R. Shakeshaft, Phys. Rev. A **44**, RC4110 (1991).
[13] See, for example, articles by J. H. Eberly *et al.*, M. Gavrila, and K. C. Kulander *et al.*, in *Atoms in Intense Laser Fields*, edited by M. Gavrila (Academic, Orlando, 1992); reviews of stabilization by M. V. Fedorov, Laser Phys. **3**, 219 (1993); Q. Su, *ibid.* **3**, 241 (1993).
[14] Q. Su, Ref. [13].
[15] M. R. Hermann and J. A. Fleck, Jr., Phys. Rev. A **38**, 6000 (1988); K. J. Schafer and K. C. Kulander, *ibid.* **42**, 5794 (1990).
[16] R. Grobe and M. V. Fedorov, J. Phys. B **26**, 1181 (1993).
[17] R. Grobe and M. V. Fedorov, Phys. Rev. Lett. **68**, 2592 (1992).
[18] For an introduction, see J. H. Eberly and K. C. Kulander, Science **262**, 1229 (1993).
[19] The "critical" laser intensity corresponding to $\alpha=2$ would be proportionally smaller than quoted here if the photon frequency were smaller, i.e., if the laser period were much longer and closer to the optical range. There is no fundamental factor that has led to the high-frequency choice $\omega=0.3$ in this paper, only considerations of required computer time, which is practically proportional to the laser period.
[20] V. C. Reed, P. L. Knight, and K. C. Burnett, Phys. Rev. Lett. **67**, 1415 (1992).